A&A, 697, A74 (2025)
https://doi.org/10.1051/0004-6361/202553930

Astronomy & Astrophysics

Evolution of massive quiescent galaxies via envelope accretion

Carlo Nipoti*

Dipartimento di Fisica e Astronomia "Augusto Righi", Alma Mater Studiorum – Università di Bologna, Via Gobetti 93/2, 40129 Bologna, Italy

Received 28 January 2025 / Accepted 28 March 2025

ABSTRACT

Aims. Massive quiescent galaxies at high redshift are significantly more compact than their present-day counterparts. We investigate the roles, in determining this evolution, of major and minor mergers, and of the accretion of diffuse envelopes of stars and dark matter.
Methods. We model the evolution in stellar mass ($M_\star$), effective radius (R_e), and effective stellar velocity dispersion (σ_e) of a representative massive quiescent galaxy from $z \approx 3$ to $z \approx 0$, and compare the model with the observed redshift-dependent R_e-$M_\star$ and σ_e-$M_\star$ relations. In the model we account for the effects of collisionless (dry) major (satellite-to-main galaxy mass ratio $\xi > 1/4$) and minor ($1/10 < \xi < 1/4$) mergers, using analytic recipes consistent with the results of N-body simulations of binary mergers. For the poorly constrained mini mergers ($\xi < 1/10$) we explore both a 'standard' model (based on the same assumptions used in the case of higher-ξ mergers), and a heuristic 'envelope accretion' model, aimed at describing the case in which diffuse satellites are completely disrupted in the galaxy outskirts.
Results. Major and minor dry mergers, at rates estimated observationally from galaxy-pair counts, induce relatively small variations in R_e and σ_e, accounting only for ≈6% of the size evolution and ≈40% of the velocity-dispersion evolution observed from $z \approx 3$ to $z \approx 0$. As an addition to major and minor dry mergers, envelope accretion performs better than standard mini mergers at reproducing the redshift dependence of the R_e-$M_\star$ and σ_e-$M_\star$ relations, being also consistent with plausible evolutionary scenarios of scaling relations involving the mass of the central supermassive black hole.

Key words. galaxies: elliptical and lenticular, cD – galaxies: evolution – galaxies: formation – galaxies: kinematics and dynamics – galaxies: structure

1. Introduction

The effective radius, R_e, and the central stellar velocity dispersion, σ_0, of present-day massive quiescent galaxies (or early-type galaxies; ETGs) correlate with the galaxy total stellar mass, $M_\star$ (Shen et al. 2003; Hyde & Bernardi 2009). These empirical scaling relations are found to evolve with redshift, z, at least out to $z \approx 2$–3: the evolution is such that, at given $M_\star$, quiescent galaxies at higher redshift have, on average, systematically smaller R_e (e.g. van der Wel et al. 2014; Martorano et al. 2024) and higher σ_0 (e.g. van de Sande et al. 2013; Cannarozzo et al. 2020, but see also Damjanov et al. 2022). Recent observations with the *James Webb Space Telescope* revealed that the size evolution of quiescent galaxies occurs also at earlier times, being possibly even stronger at redshift higher than 3 (Ito et al. 2024; Ji et al. 2024; Weibel et al. 2025; Wright et al. 2024).

The main mechanism that is believed to be responsible for this observed size and velocity-dispersion evolution is the growth of individual galaxies via dissipationless (dry) merging, which has the effect of increasing R_e linearly or super-linearly with $M_\star$, while keeping constant or decreasing σ_0 (Nipoti et al. 2003; Naab et al. 2009; Hilz et al. 2012, 2013).

The observed size evolution is however so strong that it is hard to explain only with dry merging (Nipoti et al. 2009a), also for merger histories with mass ratios and rates expected from cosmological simulations (Cimatti et al. 2012; Nipoti et al. 2012). Observational estimates of the galaxy merger rates based on measurements of the fraction of galaxy pairs are now available over wide redshift ranges (Conselice et al. 2022; Duan et al. 2024). For $z \lesssim 3$, Conselice et al. (2022), comparing their results with those of the Illustris cosmological simulation (Vogelsberger et al. 2014), find that the theoretically predicted merger rates (Rodriguez-Gomez et al. 2015) overestimate the actual merger rates, at least for mergers with mass ratio[1] $\xi > 1/10$, even though the corresponding theoretically predicted stellar mass accretion rate is lower than the observational estimate (see also Mundy et al. 2017). This makes even more puzzling the interpretation of the strong observed size evolution of passive galaxies.

In this paper we compare the observed evolution of the R_e-$M_\star$ and σ_0-$M_\star$ relations of ETGs with the predictions of dry-merging models, using observationally motivated merger mass growth rates for major ($\xi > 1/4$) and minor ($1/10 < \xi < 1/4$) mergers. We then explore quantitatively the role of mini mergers ($\xi < 1/10$), for which we have recently started to have substantial observational evidence (Suess et al. 2023). The effect of mini mergers depends on the poorly constrained properties of the involved satellites. If they are very diffuse, the cumulative effect of mini merger is expected to be an 'envelope accretion', that is the acquisition of loosely bound stars and dark matter (DM) in the galaxy outskirts (as originally envisaged by Oser et al. 2010).

Present-day ETGs lie also on scaling relations involving the mass of their central supermassive black hole (BH), $M_\bullet$, which is found to scale linearly with $M_\star$ (Magorrian et al. 1998), and with σ_0 as a power law with index 4–5 (Ferrarese & Merritt 2000; Gebhardt et al. 2000). The evolution of these scaling relations is

* Corresponding author: carlo.nipoti@unibo.it

[1] We define the merger mass ratio, $\xi \leq 1$, as the ratio between the mass of the less massive galaxy and that of the more massive galaxy.

poorly constrained observationally, because of the difficulty of measuring BH masses in higher-z ETGs. However, an indication of the masses of central BHs in high-z quiescent galaxies comes from measurements of BH masses in the so-called relic galaxies (Trujillo et al. 2014), which are compact, massive present-day quiescent galaxies with old stellar populations, believed to be descendants of high-z compact galaxies that evolved passively down to $z = 0$ without merging with other galaxies (see also Hartmann et al. 2025). Relic galaxies tend to have central BHs that are 'overmassive' (i.e. much more massive than expected for their stellar mass), but in line with the expectations for their high stellar velocity dispersion (e.g. Comerón et al. 2023). The hypothesis that high-z ETGs host overmassive BHs seems supported by the finding that, for galaxies hosting active galactic nuclei, the ratio $M_\bullet/M_\star$ was higher at $1 \lesssim z \approx 3$ than today (Mezcua et al. 2024). Instead, at least with currently available observations, there is no evidence for evolution of the $M_\bullet$-σ_0 correlation (Shen et al. 2015). The $M_\bullet$-$M_\star$ and $M_\bullet$-σ_0 relations and their evolution represent a complementary tool to test galaxy evolution models (Ciotti & van Albada 2001; Nipoti et al. 2003; Ciotti et al. 2007). We thus compared the models discussed in this work also including information on the central BH mass.

Finally, another evolutionary path of quiescent galaxies is that their central DM fraction (for instance measured within R_e) tends to increase as cosmic time goes on (Mendel et al. 2020; Damjanov et al. 2022; Tortora & Napolitano 2022). Any successful model of the evolution of ETGs must account also for this trend, which we thus took into account in our analysis.

This paper is organized as follows. In Sect. 2 we report the relevant observational data. In Sect. 3 we introduce a theoretical description of the expected effect of dry mergers on the relevant galaxy properties. The predictions for mergers with mass ratio $\xi > 1/10$ are compared with observations in Sect. 4. Sections 5 and 6 consider the contribution of mini mergers ($\xi < 1/10$). The evolution of the BH mass and DM fraction is discussed in Sect. 7. Sect. 8 concludes.

2. Observational data

Here we describe the redshift-dependent observed scaling relations that we considered in the present work, as well as the relevant observational estimates of the merger mass growth rate for massive galaxies. We limited ourselves to the redshift interval $0 \lesssim z \lesssim 3$, over which the scaling relations are relatively well characterized and over which Conselice et al. (2022) provides information on the observational estimates of the major and minor merger rates.

2.1. Redshift-dependent size-stellar mass relation

We took as reference for the observed size-stellar mass relation of ETGs the work of van der Wel et al. (2014), who find that the redshift dependence of the median correlation can be written as

$$\log\left(\frac{R_\mathrm{e}}{\mathrm{kpc}}\right) = \log A(z) + \beta(z)\log\left(\frac{M_\star}{5\times10^{10}\,\mathrm{M}_\odot}\right), \quad (1)$$

where the dimensionless redshift-dependent coefficients A and β are tabulated[2] in van der Wel et al. (2014) for $z = 0.25, 0.75, 1.25, 1.75, 2.25, 2.75$. While the logarithmic slope, β, is weakly dependent on z (with $0.7 \lesssim \beta \lesssim 0.8$), the normalization, A, depends strongly on z as

$$A \propto (1+z)^{-1.48}. \quad (2)$$

[2] The coefficient β is called α in van der Wel et al. (2014).

The above size-mass relation is plotted for different values of z in the upper panel of Fig. 1, where the curves for $z = 0$ and $z = 3$ were obtained by adopting, respectively, the same values of β as for $z = 0.25$ and $z = 2.75$, and extrapolating A from, respectively, $z = 0.25$ and $z = 2.75$, using Eq. (2). The figure also shows the intrinsic scatter of the $z = 0$ and $z = 3$ relations, assumed to be the same as that reported by van der Wel et al. (2014) at $z = 0.25$ and $z = 2.75$, respectively.

The redshift dependence of the R_e-$M_\star$ relation of ETGs has been studied by various authors. For massive ETGs Dimauro et al. (2019) and Martorano et al. (2024) find a variation with z in R_e at given $M_\star$ consistent with that estimated by van der Wel et al. (2014). A somewhat weaker evolution of R_e is found by Mowla et al. (2019) and Nedkova et al. (2021). Suess et al. (2019) and Miller et al. (2023) argue that, due to the presence of color gradients, the redshift dependence of the half-mass radius of massive quiescent galaxies is weaker than estimated by van der Wel et al. (2014), but this claim has been recently questioned by van der Wel et al. (2024). In any case, the studies that report weaker size evolution find, compared to van der Wel et al. (2014), at most 25% smaller variation in R_e at given $M_\star$ over the redshift range $0 \lesssim z \lesssim 3$. We account for this uncertainty when comparing models with observations in Sect. 4.

2.2. Redshift-dependent velocity-dispersion stellar mass relation

When considering the central stellar velocity dispersion, it is important to specify the aperture within which it is measured. Hereafter, we indicate with σ_e the effective velocity dispersion, that is the central velocity dispersion measured within an aperture that can be approximated by a circular aperture of radius R_e.

We took as reference for the observed redshift-dependent σ_e-$M_\star$ relation of ETGs the results of Cannarozzo et al. (2020), and in particular their extended-sample, constant-slope non-evolving scatter model, for which the median σ_e is given by

$$\log\left(\frac{\sigma_\mathrm{e}}{\mathrm{km\,s^{-1}}}\right) \simeq 2.21 + 0.18\log\left(\frac{M_\star}{10^{11}\,\mathrm{M}_\odot}\right) + 0.48\log(1+z). \quad (3)$$

Though this fit was obtained for galaxies in the redshift range $0 \lesssim z \lesssim 2.5$, we extrapolated it out to $z = 3$ when plotting, in the lower panel of Fig. 1, the median σ_e-$M_\star$ curves for the same selection of redshifts as in the upper panel of the same figure. The figure also shows the intrinsic scatter in σ_e of the $z = 0$ and $z = 3$ relations, assumed to be 0.08 dex, the redshift-independent value found by Cannarozzo et al. (2020).

As far as we know, for the redshift interval here considered, Cannarozzo et al. (2020) is the only work in which the σ_e-$M_\star$ relation of massive ETGs is studied systematically as a function of redshift. However, different studies have investigated whether and how σ_e depends on z for galaxies of similar $M_\star$. A few authors, consistent with Cannarozzo et al. (2020), find that σ_e at given $M_\star$ is higher at higher z (Cappellari et al. 2009; Cenarro & Trujillo 2009; van de Sande et al. 2013; Belli et al. 2017; Stockmann et al. 2020), while others find no evidence of velocity-dispersion evolution (Tanaka et al. 2019; Damjanov et al. 2022). We discuss also the hypothesis of redshift-independent σ_e-$M_\star$ relation in our analysis in Sect. 4.

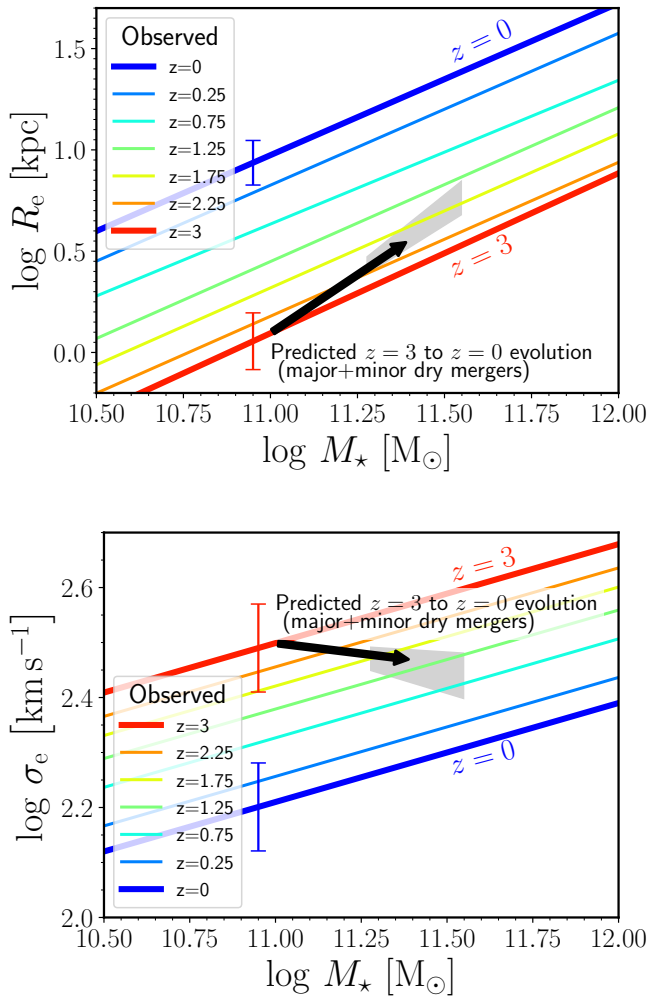

Fig. 1. ETG evolution in stellar mass, effective radius, and effective velocity dispersion, due to major and minor mergers. Upper panel: Effective radius, R_e, as a function of stellar mass, $M_\star$. The lines indicate the median observed R_e-$M_\star$ relations of ETGs at different redshifts (van der Wel et al. 2014). Lower panel: Effective stellar velocity dispersion, σ_e, as a function of stellar mass, $M_\star$. The lines indicate the median observed σ_e-$M_\star$ relations of ETGs at different redshifts (Cannarozzo et al. 2020). In each panel the black arrow indicates the predicted evolution of a representative model ETG from $z = 3$ (tail of the arrow) to $z = 0$ (head of the arrow), under the effect of major ($\xi > 1/4$) and minor ($1/10 < \xi < 1/4$) dissipationless mergers occurring at the rates observationally estimated by Conselice et al. (2022). The grey area represents the uncertainty in the position of the head of the arrow. The blue and red error bars indicate the intrinsic scatter of the scaling relations at $z = 0$ and $z = 3$, respectively.

2.3. Observed major- and minor-merger mass growth rates

Conselice et al. (2022) measured the galaxy pair and merger fractions as functions of redshift and stellar mass ratio for a large sample of massive galaxies in the redshift range $0 < z < 3$. Based on their merger rate estimates (which probe as minimum mass ratio $\xi = 1/10$), they find that galaxies with stellar mass $M_\star > 10^{11}\,\mathrm{M}_\odot$, from $z = 3$ to $z = 0$, grow in stellar mass by $f_{\rm maj} = 93^{+49}_{-31}\%$ via major mergers ($\xi > 1/4$) and by $f_{\rm min} = 29^{+17}_{-12}\%$ via minor mergers ($1/10 < \xi < 1/4$). It is worth noting that these estimates are based on a stellar-mass selection; when Conselice et al. (2022) apply instead a constant-number density selection, they find significantly lower stellar-mass growth rates for both major and minor mergers. In the spirit of maximizing the possible effect of mergers on the evolution of the scaling relations, in our analysis we assumed that, on average, from $z = 3$ to $z = 0$ massive ETGs increase their stellar mass by the aforementioned values of $f_{\rm maj}$ and $f_{\rm min}$, for major and minor mergers, respectively. It is important to stress that the contribution of mini mergers ($\xi < 1/10$) is not included in these numbers.

Before Conselice et al. (2022), other authors attempted to measure the merger rate of massive galaxies at $z \lesssim 3$, accounting for the contribution of major and minor mergers. Bluck et al. (2012) estimate that, from $z = 3$ to the present (see also López-Sanjuan et al. 2011), galaxies of $M_\star \sim 10^{11}\,\mathrm{M}_\odot$, via mergers with mass ratio $\xi > 1/100$, undergo a fractional stellar-mass increase 2.0 ± 1.2, which, within the relatively large uncertainty, is consistent with the estimate of Conselice et al. (2022). A somewhat lower stellar mass growth due to $\xi > 1/10$ mergers ($\approx$50% from $z = 2.5$ to $z = 0$) is instead estimated by Man et al. (2016). Similar results are reported by Newman et al. (2012), who find merger rates consistent with those of Man et al. (2016) in the redshift range $0.4 < z < 2.5$.

3. Effect of dry mergers on R_e and σ_e

The effects of mergers on the galactic structural and kinematic properties depend in a complex way on the internal properties of the interacting galaxies, on their mass ratio and on the characteristics of their mutual orbits (see section 8.9 of Cimatti et al. 2019).

Even limiting to the case of gas-poor spheroidal galaxies, the variations in R_e and σ_e produced by mergers depend not only on the merger mass ratio, but also on the orbital parameters of the encounter and on the internal distribution of stars and DM of the interacting systems. However, some general physical arguments can be used to obtain approximate analytic predictions for the evolution of R_e and σ_e in dry merging.

3.1. Analytic formulae

Under the assumption that $R_e \propto r_g$ and $\sigma_e \propto \sigma_{\rm vir}$, where r_g is the gravitational radius and $\sigma_{\rm vir}$ is the virial velocity dispersion, the effect of dry mergers on R_e and σ_e can be computed using energy conservation and the virial theorem (Nipoti et al. 2003; Naab et al. 2009; Hilz et al. 2012). In particular, in the case of parabolic orbits, under these hypotheses, for a galaxy growing with a sequence of dry mergers with mass ratio ξ, R_e and σ_e grow with stellar mass as, respectively,

$$R_e \propto {M_\star}^{\alpha_R(\xi)} \tag{4}$$

and

$$\sigma_e \propto {M_\star}^{\alpha_\sigma(\xi)}, \tag{5}$$

with

$$\alpha_R(\xi) = 2 - \frac{\ln(1+\xi^{2-\beta_R})}{\ln(1+\xi)} \tag{6}$$

and

$$\alpha_\sigma(\xi) = -\frac{1}{2}\left[1 - \frac{\ln(1+\xi^{2-\beta_R})}{\ln(1+\xi)}\right] \tag{7}$$

(Nipoti et al. 2012), where we have assumed that the merging galaxies lie on a size-mass relation $R_e \propto {M_\star}^{\beta_R}$.

3.2. Range of validity of the analytic formulae for major, minor, and mini mergers

There are a few works in the literature in which the evolution of the effective radius and of the central velocity dispersion in dissipationless mergers has been studied with N-body simulations (Nipoti et al. 2003, 2009b, 2012; Boylan-Kolchin et al. 2006; Hilz et al. 2012, 2013; Frigo & Balcells 2017; Rantala et al. 2024). The simulations run in these works differ widely in mass ratio, orbital parameters, and internal properties of the interacting systems (such as amount and distribution of dark and baryonic matter), and consequently also the behaviour of R_e and σ_e shows a relatively wide variety. However, trying to make a synthesis of the results of these work, Eqs. (4)–(7) appear to describe sufficiently well the average effects of major mergers (Nipoti et al. 2003, 2009b; Boylan-Kolchin et al. 2006; Hilz et al. 2012) and of minor mergers (Nipoti et al. 2012; Frigo & Balcells 2017). In N-body simulations of equal-mass mergers the central velocity dispersion tends to increase slightly, but the deviation from the constant-σ_e prediction of Eq. (7) is typically within 15% (Nipoti et al. 2003, 2009b; Boylan-Kolchin et al. 2006; Hilz et al. 2012). Rantala et al. (2024) find that the size evolution is stronger when central BHs are included in the simulations: on average, in their numerical experiments, the index α_R is higher in the presence than in the absence of central BHs by ≈10% in major mergers and ≈30% in minor mergers (see their Table 5). Considering overall the results of the aforementioned works, we decided to use Eqs. (4)–(7) for major and minor mergers, but keeping in mind the uncertainties on α_R and α_σ.

The situation is much more uncertain for mini mergers ($\xi < 1/10$), which have been studied relatively little in the literature. As far as we know, the only systematic exploration of the effect of mini mergers on R_e and σ_e is that of Hilz et al. (2012), who simulated dry mergers with mass ratios $0.05 < \xi \leq 0.1$ in which the satellite is much less dense than the main galaxy ($0 \lesssim \beta_R \lesssim 0.3$; see also Hilz et al. 2013 and Rantala et al. 2024). Hilz et al. (2012) found significant deviations from the analytic predictions of Eqs. (4)–(7): in particular the values of α_σ found in simulations are systematically higher than those predicted by Eq. (7). Though limited to some very specific cases, the results of these numerical experiments suggest that Eqs. (4)–(7) do not necessarily capture the effects of mergers with very small mass ratios. Thus, in the attempt of bracketing the realistic behaviour, in the case of mini mergers we explored two very different scenarios: 'standard mini mergers' (Sect. 5), in which we assumed that Eqs. (4)–(7) hold, and 'envelope accretion' (Sect. 6), in which we assumed that the satellites are very diffuse and they deposit the great majority of their stars and DM in the outskirts of the main galaxy.

4. Weak evolution driven by major and minor mergers at the observed rates

Using the formulae presented in Sect. 3, we computed the evolution of individual galaxies in the $M_\star$-R_e and $M_\star$-σ_e planes, due to $\xi > 1/10$ mergers at the observed rates (Sect. 2.3), and compared it with the observed evolution of the scaling relations (Sects. 2.1 and 2.2). Given that the considered scaling relations are power laws with virtually redshift-independent slopes[3], and that the merger-driven evolution in the $M_\star$-R_e and $M_\star$-σ_e planes is modelled with power laws, the initial stellar mass of our reference galaxy can be chosen arbitrarily in the mass range in which the scaling relations have been computed.

However, to consistently use the merger mass growth rates of Conselice et al. (2022), we limited ourselves to stellar masses $M_\star \geq 10^{11}\,\mathrm{M}_\odot$. We thus considered as our 'initial galaxy' a model ETG that at $z = 3$ has $M_\star = 10^{11}\,\mathrm{M}_\odot$, $R_e \simeq 1.24\,\mathrm{kpc}$ and $\sigma_e \simeq 316\,\mathrm{km\,s^{-1}}$, values such that it lies on the $z = 3$ scaling relations shown in Fig. 1. We then modelled its evolution assuming that its stellar mass from $z = 3$ to $z = 0$ grows as

$$M_{\star,z=0} = M_{\star,z=3}(1 + f_{\rm maj})(1 + f_{\rm min}), \tag{8}$$

where $f_{\rm maj}$ and $f_{\rm min}$ are the fractional stellar mass increase[4] over the redshift range $0 < z < 3$, and the subscripts $z = 0$ and $z = 3$ indicate at which redshift the quantity is evaluated. It follows from the equations of Sect. 3 that the corresponding evolution in size and velocity dispersion is described by

$$R_{e,z=0} = R_{e,z=3}(1 + f_{\rm maj})^{\alpha_R(\xi_{\rm maj})}(1 + f_{\rm min})^{\alpha_R(\xi_{\rm min})}, \tag{9}$$

and

$$\sigma_{e,z=0} = \sigma_{e,z=3}(1 + f_{\rm maj})^{\alpha_\sigma(\xi_{\rm maj})}(1 + f_{\rm min})^{\alpha_\sigma(\xi_{\rm min})}, \tag{10}$$

respectively. Here $\xi_{\rm maj}$ and $\xi_{\rm min}$ are characteristic mass ratios for major and minor mergers, respectively, and we recall that α_R and α_σ depend also on β_R.

For our fiducial model we assumed $f_{\rm maj} = 0.93$, $f_{\rm min} = 0.29$ (Sect. 2.3), $\beta_R = 0.76$ (the median value of the R_e-$M_\star$ relation logarithmic slope, β, found by van der Wel et al. 2014; Sect. 2.1), $\xi_{\rm maj} = (1+0.25)/2 = 0.625$ and $\xi_{\rm min} = (0.1+0.25)/2 = 0.175$. With these parameters we obtained $\delta \log M_\star = 0.40$, $\delta \log R_e = 0.46$ and $\delta \log \sigma_e = -0.03$, where we have introduced the notation $\delta q = q(z = 0) - q(z = 3)$, to indicate the variation in a generic quantity q for an individual galaxy. In Fig. 1 the black arrows indicate this predicted evolution for our fiducial galaxy in the $M_\star$-R_e plane (upper panel) and $M_\star$-σ_e plane (lower panel), with the head of the arrow indicating the predicted position at $z = 0$ due to major and minor mergers only. In each panel, the grey shaded area indicates the uncertainty in the position of the head of the arrow. We computed this area considering the uncertainties on $f_{\rm maj}$ and $f_{\rm min}$ (Sect. 2.3), as well as those on α_R and α_σ, which we approximately accounted for by allowing $\xi_{\rm maj}$ and $\xi_{\rm min}$ to vary, respectively, in the ranges $1/4 \leq \xi_{\rm maj} \leq 1$ and $1/10 \leq \xi_{\rm min} \leq 1/4$, and β_R in the range $0.7 \leq \beta_R \leq 0.8$ (Sect. 2.1).

The result shown by the upper panel of Fig. 1 is striking: major and minor mergers at the observed rates are expected to produce a weak size evolution from $z = 3$ to $z = 0$, much less than the observed evolution of the size-mass relation over the same redshift interval (even if the intrinsic scatter of the relations and the uncertainty in the position of the head of the arrow are taken into account). Our representative model galaxy at redshift $z = 0$ (head of the arrow in the plot) has stellar mass $\simeq 2.5 \times 10^{11}\,\mathrm{M}_\odot$ and effective radius $R_e \simeq 3.6\,\mathrm{kpc}$, about a factor of five smaller than the average R_e of observed $z = 0$ ETGs of similar stellar mass. This finding confirms and strengthens the results of

[3] While the slope of the considered σ_e-$M_\star$ relation is strictly independent of z (Cannarozzo et al. 2020), the slope of the R_e-$M_\star$ relation of van der Wel et al. (2014) varies only very slightly with z (see their Table 1).

[4] These quantities can be to a good approximation identified with the ratios $\delta M_{\rm maj,\star}/M_0$ and $\delta M_{\rm min,\star}/M_0$ computed by Conselice et al. (2022), because in that paper M_0 is the average mass ($M_\star \approx 1.6 \times 10^{11}\,\mathrm{M}_\odot$) of the massive galaxy population in the redshift interval $0 < z < 3$.

Newman et al. (2012) and Man et al. (2016), who reported that the observed merger rates are insufficient to explain the strong size evolution of massive quiescent galaxies.

The lower panel of Fig. 1 shows that also the predicted evolution of the velocity dispersion is too weak: the σ_e of the model galaxy decreases slowly, with a final value as high as $\simeq$294 km s^{-1}, about 50% higher than the median σ_e of observed $z = 0$ ETGs of similar stellar mass. However, different from the size evolution, the predicted velocity-dispersion evolution is marginally consistent with the observations if the intrinsic scatter of the relations and the uncertainty in the position of the head of the arrow are taken into account.

To quantify the relative contribution of major and minor mergers to the size and velocity-dispersion evolution from $z = 3$ to $z = 0$, it is convenient to define the offsets

$$\Delta R_{\rm e,obs} = |R_{\rm e,obs}(M_{\star,\rm maj+min}, 0) - R_{\rm e,obs}(M_{\star,\rm maj+min}, 3)|, \quad (11)$$

$$\Delta R_{\rm e,maj+min} = |R_{\rm e,maj+min} - R_{\rm e,obs}(M_{\star,\rm maj+min}, 3)|, \quad (12)$$

$$\Delta \sigma_{\rm e,obs} = |\sigma_{\rm e,obs}(M_{\star,\rm maj+min}, 0) - \sigma_{\rm e,obs}(M_{\star,\rm maj+min}, 3)|, \quad (13)$$

and

$$\Delta \sigma_{\rm e,maj+min} = |\sigma_{\rm e,maj+min} - \sigma_{\rm e,obs}(M_{\star,\rm maj+min}, 3)|, \quad (14)$$

where $R_{\rm e,obs}(M_\star, z)$ and $\sigma_{\rm e,obs}(M_\star, z)$ are, respectively, the observed R_e-$M_\star$ and σ_e-$M_\star$ correlations (Sects. 2.1 and 2.2), and $M_{\star,\rm maj+min}$, $R_{\rm e,maj+min}$, and $\sigma_{\rm e,maj+min}$ are the values of $M_\star$, R_e, and σ_e predicted at $z = 0$ by a model accounting only for major and minor mergers (corresponding to the heads of the arrows in Fig. 1). Over the range $0 < z < 3$, the contribution of major and minor mergers is $\Delta R_{\rm e,maj+min}/\Delta R_{\rm e,obs} \simeq 6\%$ to the size evolution and $\Delta \sigma_{\rm e,maj+min}/\Delta \sigma_{\rm e,obs} \simeq 42\%$ to the velocity-dispersion evolution.

We have mentioned in Sects. 2.1 and 2.2 that, according to some authors, the evolution in R_e and σ_e at given $M_\star$ could be weaker than estimated by van der Wel et al. (2014) and Cannarozzo et al. (2020). Even assuming that $R_{\rm e,obs}(M_{\star,\rm maj+min}, 0)$ is smaller by 25% (see Sect. 2.1), $\Delta R_{\rm e,maj+min}/\Delta R_{\rm e,obs}$ is as small as $\approx$8%. The evolution of the σ_e-$M_\star$ relation is much more uncertain and debated in the literature, so it is not excluded that $\Delta \sigma_{\rm e,maj+min}/\Delta \sigma_{\rm e,obs}$ is closer to unity than found using the z-dependent scaling relation of Cannarozzo et al. (2020), which is however the state of the art with currently available datasets. The result that $\Delta R_{\rm e,maj+min}/\Delta R_{\rm e,obs}$ is small is robust also against uncertainties on the value α_R: even if, following Rantala et al. (2024), we increase α_R by 10% for major mergers and by 30% for minor mergers (see Sect. 3.2), we get $\Delta R_{\rm e,maj+min}/\Delta R_{\rm e,obs} \approx 11\%$.

In this section we have estimated the predicted evolution due only to mergers with mass ratio $\xi > 1/10$. To this evolution we must add the contribution of mergers with $\xi < 1/10$, which we consider in Sects. 5 and 6.

5. Standard mini dry mergers

As pointed out in Sect. 3, the effect on R_e and σ_e of mass growth via mini ($\xi < 1/10$) mergers is poorly constrained. When considering growth via mini mergers we thus explored two different simple scenarios. In this section we consider standard mini mergers, while in Sect. 6 we consider envelope accretion. With standard mini mergers we mean parabolic $\xi < 1/10$ dry mergers such that $R_e \propto r_g$ and $\sigma_e \propto \sigma_{\rm vir}$, so that the formulae of Sect. 3 apply. Given the uncertainty on the dominant mass ratio of mini mergers and the fact that the observed evolution of the R_e-$M_\star$ relation is strong (Fig. 1, upper panel), to maximize the size evolution we model here mini mergers as dry mergers with vanishingly small mass ratio. In the considered hypotheses, taking the limit for $\xi \to 0$ of Eqs. (4) and (5) we get[5] $R_e \propto {M_\star}^2$ and $\sigma_e \propto {M_\star}^{-1/2}$ (Naab et al. 2009). In Fig. 2 we show the evolution in the $M_\star$-R_e (upper panel) and $M_\star$-σ_e (lower panel) planes of our representative model galaxy when, to the contribution of major and minor mergers (Sect. 4), we add a contribution of standard mini mergers such that our model galaxy lies on the median R_e-$M_\star$ relation of ETGs at $z = 0$. To achieve this, our model galaxy grows in stellar mass by almost a factor of 10 from $z = 3$ to $z = 0$ (including major, minor, and mini mergers). The required fractional mass growth due to mini mergers is thus $f_{\rm mini} \approx 2.6$.

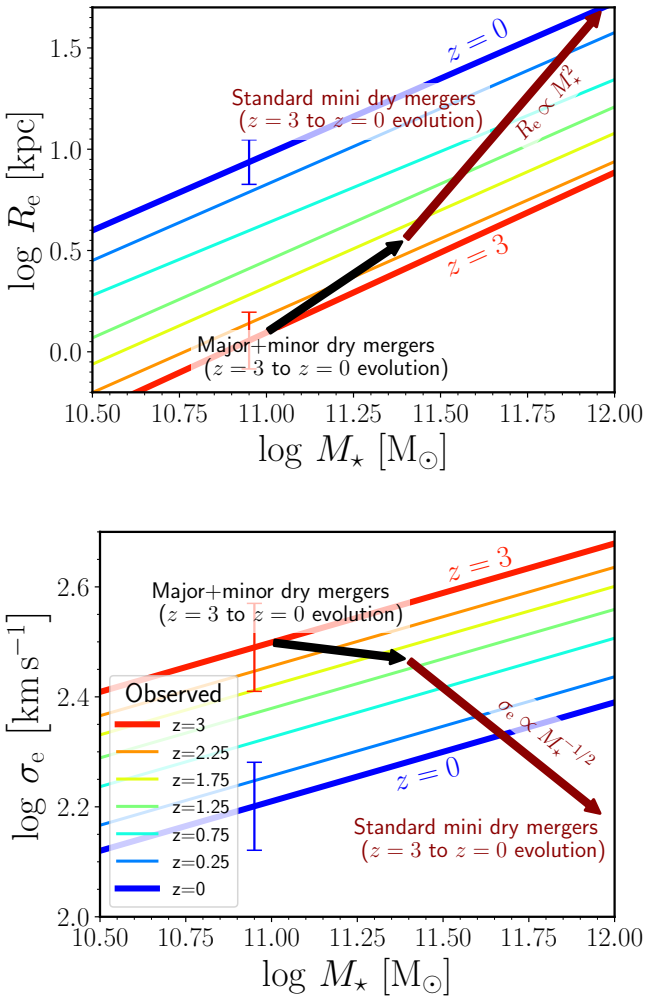

Fig. 2. ETG evolution in stellar mass, effective radius, and effective velocity dispersion, due to major, minor, and standard mini mergers. Same as Fig. 1, but with the addition of the potential contribution from $z = 3$ to $z = 0$ of standard mini dry mergers (red arrows), that is mergers with $\xi \ll 1$ in which R_e and σ_e vary with stellar mass as $R_e \propto {M_\star}^2$ and $\sigma_e \propto {M_\star}^{-1/2}$, respectively. These power laws are the limits of Eqs. (4) and (5) for $\xi \to 0$ (independent of β_R, provided $\beta_R < 1$). While the stellar mass growth attributed to major and minor mergers (black arrows) is based on observational estimates (Sect. 2.3), the stellar mass growth attributed to mini mergers (red arrows) is chosen ad hoc so that in the upper panel the head of the red arrow lies on the observed $z = 0$ R_e-$M_\star$ correlation.

[5] In fact, this is true provided $\beta_R < 1$, which is however a standard assumption, generally supported by the observations.

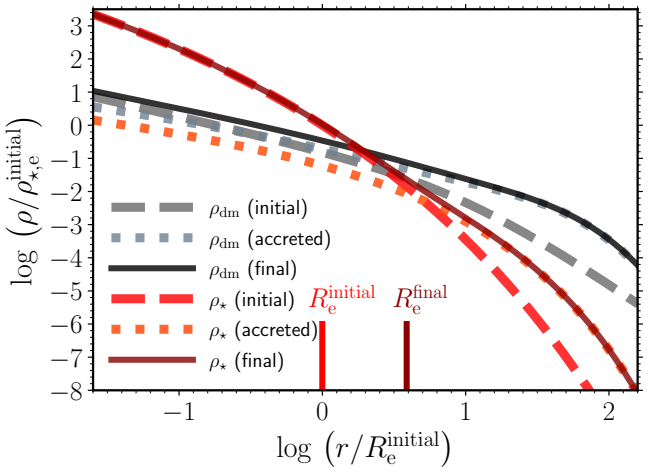

Fig. 3. Envelope accretion-driven evolution of the density distribution of a representative ETG. Initial (dashed curves), accreted (dotted curves), and final (solid curves) stellar (red curves) and DM (black and grey curves) density profiles of our reference model galaxy growing via envelope accretion. The vertical lines indicate the initial ($R_{\mathrm{e}}^{\mathrm{initial}}$) and final ($R_{\mathrm{e}}^{\mathrm{final}}$) effective radii. $\rho_{\star,\mathrm{e}}^{\mathrm{initial}}$ is the initial stellar density at $r = R_{\mathrm{e}}^{\mathrm{initial}}$.

The lower panel of Fig. 2 shows that the same model galaxy is predicted to have way too low σ_{e} at $z = 0$.

In Fig. 2 we show as example of evolution driven by standard mini mergers only the case with vanishingly small mass ratio ($\xi \to 0$), which maximizes the increase in R_{e} and the decrease in σ_{e} for given stellar mass growth. If, instead of $\xi \to 0$, we assumed for our standard mini-merger model as characteristic mass ratio a more realistic finite value $\xi < 1/10$, we would get red arrows with shallower slope in both panels of Fig. 2. However, this would not help solve the problem of the too low predicted σ_{e} at $z = 0$, because higher stellar mass growth via mini mergers would be required to match the $z = 0$ R_{e}-$M_\star$ relation, and thus too low values of σ_{e} at $z = 0$ would be predicted even with a shallower predicted evolution in the $M_\star$-σ_{e} plane.

We recall that in Sect. 3 (and thus in the standard mini merger model here considered), we assumed not only that R_{e} and σ_{e} are proportional, respectively, to the gravitational radius and virial velocity dispersion, but also that the mergers are parabolic. If the orbital energy is negative, the final velocity dispersion can be higher than in the parabolic case (Nipoti et al. 2009b; Posti et al. 2014). However, the more bound the orbits, the weaker is the size growth, so it seems unlikely that adding the effects of negative orbital energy can help produce, at the same time, the needed strong evolution in R_{e} and the relatively weak evolution of σ_{e}, within the framework of standard mini mergers. A more promising solution is the accretion of very diffuse satellites, which we discuss in the next section.

6. Envelope accretion

We consider here the case in which in mini mergers the accreted material ends up in an envelope, that is a diffuse, extended component.

6.1. A toy model for envelope accretion

We built a toy model for envelope accretion by considering an initial galaxy model (representing a higher-z quiescent galaxy) and a final galaxy model (representing its lower-z descendant) obtained by simply adding to the initial galaxy model an accreted stellar component and an accreted DM component. The models, which are spherically symmetric, were computed following the approach of Nipoti et al. (2008). The initial galaxy has stellar density $\rho_\star^{\mathrm{initial}}(r)$ and DM density $\rho_{\mathrm{dm}}^{\mathrm{initial}}(r)$; the final galaxy has stellar density $\rho_\star^{\mathrm{final}}(r) = \rho_\star^{\mathrm{initial}}(r) + \rho_\star^{\mathrm{accr}}(r)$ and DM density $\rho_{\mathrm{dm}}^{\mathrm{final}}(r) = \rho_{\mathrm{dm}}^{\mathrm{initial}}(r) + \rho_{\mathrm{dm}}^{\mathrm{accr}}(r)$, where $\rho_\star^{\mathrm{accr}}$ and $\rho_{\mathrm{dm}}^{\mathrm{accr}}$ are, respectively, the stellar and DM accreted mass density. We now define the functional forms that we use to model $\rho_\star^{\mathrm{initial}}$, $\rho_{\mathrm{dm}}^{\mathrm{initial}}$, $\rho_\star^{\mathrm{accr}}$, and $\rho_{\mathrm{dm}}^{\mathrm{accr}}$.

6.1.1. Stellar components

Both the initial and the accreted stellar components are described by Sérsic (1968) models. The projected density distribution follows the Sérsic $R^{1/m}$ law

$$\Sigma_\star(R) = \Sigma_{\star,0}\,\exp\left[-b(m)\left(\frac{R}{R_{\mathrm{e}}}\right)^{1/m}\right], \tag{15}$$

where $b(m) \approx 2m - 1/3 + 4/(405m)$ (Ciotti & Bertin 1999) and m is the so-called Sérsic index. By deprojecting $\Sigma_\star$ one obtains the corresponding intrinsic density distribution (Binney & Tremaine 2008)

$$\rho_\star(r) = -\frac{1}{\pi}\int_r^\infty \frac{\mathrm{d}\Sigma_\star}{\mathrm{d}R}\frac{\mathrm{d}R}{\sqrt{R^2 - r^2}}, \tag{16}$$

which we computed numerically.

6.1.2. Dark-matter components

The DM halo of the initial galaxy is described by a Navarro et al. (1996) model, with density distribution

$$\rho_{\mathrm{dm}}^{\mathrm{initial}}(r) = 4\rho_{\mathrm{s}}\left(\frac{r}{r_{\mathrm{s}}}\right)^{-1}\left(\frac{r}{r_{\mathrm{s}}} + 1\right)^{-2}, \tag{17}$$

where r_{s} is the scale radius and $\rho_{\mathrm{s}} \equiv \rho_{\mathrm{dm}}^{\mathrm{initial}}(r_{\mathrm{s}})$.

The dark accreted component is assumed to have a density distribution

$$\rho_{\mathrm{dm}}^{\mathrm{accr}}(r) = \Xi^{\mathrm{accr}}\rho_\star^{\mathrm{accr}}(r)\left(1 + \frac{r}{R_{\mathrm{e}}^{\mathrm{accr}}}\right)^3, \tag{18}$$

where $R_{\mathrm{e}}^{\mathrm{accr}}$ is the projected half-mass radius of the accreted stellar component and Ξ^{accr} is a dimensionless factor such that, for given $\rho_\star^{\mathrm{accr}}(r)$, the DM-to-stellar mass ratio of the accreted material increases for increasing Ξ^{accr}.

6.1.3. Stellar mass, effective radius, and central velocity dispersion

For both the initial and final galaxy models we need the total mass, the effective radius, and the effective stellar velocity dispersion. The total stellar mass was obtained by computing numerically the integral

$$M_\star = 4\pi\int_0^\infty \rho_\star(r) r^2 \mathrm{d}r. \tag{19}$$

The value of R_{e} is such that $M_\star^{\mathrm{p}}(R_{\mathrm{e}}) = M_\star/2$, where

$$M_\star^{\mathrm{p}}(R) = 2\pi\int_0^R \Sigma_\star(R')R'\,\mathrm{d}R' \tag{20}$$

is the projected stellar mass within R and $\Sigma_\star(R)$ is the total stellar surface density.

Assuming isotropic velocity distribution, the radial component $\sigma_r(r)$ of the velocity dispersion tensor was obtained by solving the Jeans equation

$$\frac{\mathrm{d}\left(\rho_\star\sigma_r^2\right)}{\mathrm{d}r} = -\rho_\star\frac{\mathrm{d}\Phi}{\mathrm{d}r}, \tag{21}$$

where $\Phi(r)$ is the total gravitational potential generated by the total density distribution $\rho_{\rm tot} = \rho_\star + \rho_{\rm dm}$.

For the considered isotropic systems, the line-of-sight velocity dispersion squared is (Binney & Mamon 1982)

$$\sigma^2_{\rm los}(R) = \frac{2}{\Sigma_\star(R)}\int_R^\infty \frac{\rho_\star(r)\sigma_r^2 r\mathrm{d}r}{\sqrt{r^2-R^2}}. \tag{22}$$

The aperture velocity dispersion $\sigma_{\rm a}$ within a projected radius R was determined via

$$\sigma^2_{\rm a}(R) = \frac{2\pi}{M^{\rm p}_\star(R)}\int_0^R \Sigma_\star(R')\sigma^2_{\rm los}(R')R'\mathrm{d}R'. \tag{23}$$

The effective stellar velocity dispersion is $\sigma_{\rm e} \equiv \sigma_{\rm a}(R_{\rm e})$.

6.2. A reference case

We present here a specific example of the toy model for envelope accretion described in Sect. 6.1. We will take this specific example as a reference case to illustrate quantitatively possible effects of envelope accretion on the evolution of ETGs in the space of the parameters $M_\star$, $R_{\rm e}$, and $\sigma_{\rm e}$. For our purposes we do not need to work in physical units, but we can take as reference mass and length units, respectively, the stellar mass, $M_\star^{\rm initial}$, and the effective radius, $R_{\rm e}^{\rm initial}$, of the initial galaxy model. As it is natural, we adopt as velocity unit $v_{\rm u} = \left(GM_\star^{\rm initial}/R_{\rm e}^{\rm initial}\right)^{1/2}$.

The initial galaxy model has stellar density profile given by the equations of Sect. 6.1.1 with effective radius $R_{\rm e} = R_{\rm e}^{\rm initial}$, $m = 4$, and $\Sigma_{\star,0}$ such that $M_\star = M_\star^{\rm initial}$. Its DM density profile is given by the equations of Sect. 6.1.2 with $r_{\rm s} = 10R_{\rm e}^{\rm initial}$ and $\rho_{\rm s}$ such that $f_{\rm dm,e} = 0.05$, where

$$f_{\rm dm,e} \equiv \frac{M_{\rm dm}(R_{\rm e})}{M_\star(R_{\rm e}) + M_{\rm dm}(R_{\rm e})} \tag{24}$$

is the DM fraction within a sphere of radius $R_{\rm e}$. Here $M_\star(r)$ and $M_{\rm dm}(r)$ are, respectively, the stellar and DM masses enclosed within a sphere of radius r. For the adopted values of the parameters, the initial effective velocity dispersion is $\sigma_{\rm e}^{\rm initial} \simeq 0.296v_{\rm u}$. The accreted component has stellar density profile given by the equations of Sect. 6.1.1 with effective radius $R_{\rm e}^{\rm accr} = 12R_{\rm e}^{\rm initial}$, $m = 2$, and $\Sigma_{\star,0}$ such that $M_\star = M_\star^{\rm accr} = M_\star^{\rm initial}$, and DM density profile given by Eq. (18) with $\Xi^{\rm accr} = 2.5$. The final galaxy model, which by construction has $M_\star^{\rm final} = M_\star^{\rm initial} + M_\star^{\rm accr} = 2M_\star^{\rm initial}$, has $R_{\rm e}^{\rm final} \simeq 3.9R_{\rm e}^{\rm initial}$ and $\sigma_{\rm e}^{\rm final} \simeq 0.293v_{\rm u} \simeq 0.99\sigma_{\rm e}^{\rm initial}$.

Fig. 3 shows the stellar and DM density profiles of the initial galaxy model (dashed curves), the accreted components (dotted curves), and the final galaxy model (solid curves). The assumed profiles are somewhat arbitrary, but we note that the relative distribution of the initial and accreted components is qualitatively similar to those found in cosmological simulations of massive galaxies (Oser et al. 2012; Cooper et al. 2013). Though the model shown in Fig. 3 is just a specific example of accretion of an extended envelope, it nicely illustrates that this process can have the effect of producing an increase in $R_{\rm e}$ similar to standard mini mergers with $\xi \to 0$, while keeping $\sigma_{\rm e}$ essentially constant, as it happens in the case of major mergers. Modelling, as in Sect. 3, the evolution of $R_{\rm e}$ and $\sigma_{\rm e}$ with $M_\star$ with power laws $R_{\rm e} \propto M_\star^{\alpha_R}$ and $\sigma_{\rm e} \propto M_\star^{\alpha_\sigma}$, for the model here considered (and shown in Fig. 3) we get

$$\alpha_R = \frac{\ln R_{\rm e}^{\rm final} - \ln R_{\rm e}^{\rm initial}}{\ln M_\star^{\rm final} - \ln M_\star^{\rm initial}} \simeq 1.96, \tag{25}$$

and

$$\alpha_\sigma = \frac{\ln \sigma_{\rm e}^{\rm final} - \ln \sigma_{\rm e}^{\rm initial}}{\ln M_\star^{\rm final} - \ln M_\star^{\rm initial}} \simeq -0.01. \tag{26}$$

6.3. Envelope accretion and scaling relations

Here we want to study the possible evolution induced by the envelope accretion in the planes $M_\star$-$R_{\rm e}$ and $M_\star$-$\sigma_{\rm e}$. Taking the model presented in Sect. 6.2 as reference to quantify the effects of envelope accretion on $R_{\rm e}$ and $\sigma_{\rm e}$, for this mechanism we assume here $R_{\rm e} \propto M_\star^{\alpha_R}$ with $\alpha_R = 2$ and $\sigma_{\rm e} \propto M_\star^{\alpha_\sigma}$ with $\alpha_\sigma = 0$ (see Eqs. (25) and (26)).

In Fig. 4 we report the result of an exercise similar to that shown in Fig. 2, but assuming that, beside major and minor mergers, the evolution of our reference ETG from $z = 3$ to $z = 0$ is due to envelope accretion instead of standard mini mergers. As done in Sect. 5 for standard mini mergers, here the assumed increase in stellar mass attributed to the envelope is such that our model galaxy lies on the median $R_{\rm e}$-$M_\star$ relation of ETGs at $z = 0$. Comparing the bottom panel of Fig. 4 with that of Fig. 2, the substantial difference in the value of the final $\sigma_{\rm e}$ in the two models is apparent. The observationally expected $z = 0$ value of $\sigma_{\rm e}$ lies above that predicted by the standard mini merger model and below that predicted by the envelope accretion model. We note that the deviation from the $z = 0$ scaling relation of the envelope accretion prediction is significantly smaller than that of the standard mini mergers model, though this result should not be taken at face value, given the highly idealized nature of the considered models. Nevertheless, this exercise shows very clearly that the envelope accretion can have an important role in the evolution of ETGs and that the effect on $\sigma_{\rm e}$ of the accretion of small satellites (corresponding to mergers with mass ratio lower than 1/10) could be quite different from the standard mini merger model, and needs to be better constrained observationally and theoretically.

Another feature of envelope accretion, which is evident from Fig. 3, is that the inner stellar density distribution is virtually unchanged during the process. This is particularly interesting in light of the fact that for massive ETGs (though so far only over the limited redshift range $0.17 < z < 0.37$) there is no evidence of redshift-dependence of the logarithmic slope of the stellar mass surface density profile within the inner 10 kpc (Liu et al. 2025).

The required fractional mass growth due to envelope accretion (see Fig. 4) is $f_{\rm env} \approx 2.6$, which, assuming our fiducial values $f_{\rm maj} = 0.93$ and $f_{\rm min} = 0.29$ (Sect. 2.3), corresponds to a ratio between envelope accretion growth and major-plus-minor merger growth $\mathcal{R} \equiv f_{\rm env}/(f_{\rm maj} + f_{\rm min}) \simeq 2.1$. This is much higher than estimated by Suess et al. (2023), who, observing satellites around massive quiescent galaxies in the redshift range $0 \leq z \leq 3$, find that the stellar mass accreted via mini mergers is ≈30% of the total accreted stellar mass (corresponding to $\mathcal{R} \approx 0.43$). However, Suess et al. (2023) stress that their

estimate must be considered a lower limit, because of expected incompleteness of their sample. A rough estimate of the maximum stellar mass potentially available for envelope accretion (relative to that for major and minor mergers) can be obtained as follows. Let us model the galaxy stellar mass function as a Schechter (1976) law with characteristic mass $M_\star^*$ and low-mass-end logarithmic slope $\alpha_{\rm SMF}$. For a galaxy of stellar mass $XM_\star^*$, the ratio between the stellar mass potentially available for mini mergers ($\xi < 0.1$) and that potentially available for major and minor mergers ($\xi > 0.1$) is

$$\mathcal{R} = \frac{\int_0^{0.1X} x^{1+\alpha_{\rm SMF}} e^{-x} {\rm d}x}{\int_{0.1X}^{X} x^{1+\alpha_{\rm SMF}} e^{-x} {\rm d}x}, \tag{27}$$

where the integration variable is $x = M_\star/M_\star^*$. For slopes in the interval $-1.8 \lesssim \alpha_{\rm SMF} \lesssim -1.3$ (as observed in the redshift range $0 < z < 3$; Davidzon et al. 2017) and $X = 3$ (i.e. for a $M_\star \sim 10^{11}\,{\rm M}_\odot$ galaxy), we get $0.8 \lesssim \mathcal{R} \lesssim 4.5$, so there is potentially room for mini-merger dominated accretion. From a theoretical point of view, an independent indication of the importance of accretion of very small satellites comes from cosmological simulations. For instance, in DM-only cosmological simulations, Fakhouri & Ma (2010) find that the ratio between mass gained in mergers with DM mass ratio $\xi < 0.1$ and that gained in $\xi > 0.1$ mergers is in the range $1.5 \lesssim \mathcal{R} \lesssim 2.3$.

7. Evolution of black-hole mass and dark-matter fraction

We discuss here the predictions of the considered model involving envelope accretion for the evolution of properties of the dark components of quiescent galaxies, namely the mass of the central supermassive BH and the central DM fraction.

7.1. Scaling relations involving the mass of the central black hole

Little is known observationally about the mass of putative central BHs in high-redshift quiescent galaxies. However, useful information in this respect comes from the study of the relic galaxies, which are believed to be rare descendants of massive compact high-z ETGs that have evolved passively since $z \gtrsim 2$. If this is indeed the case, we can assume that high-z ETGs have the same $M_\bullet$ as present-day relic galaxies of similar $M_\star$ and $\sigma_{\rm e}$.

Estimates of masses of central BHs in relic galaxies are provided by Ferré-Mateu et al. (2015, 2017) and Comerón et al. (2023). They tend to have $M_\bullet$ an order of magnitude higher than non-relic present-day galaxies of similar stellar mass. The best studied relic galaxy is NCG 1277, with $M_\star \simeq 1.8 \times 10^{11}\,{\rm M}_\odot$ (Comerón et al. 2023) and $\sigma_{\rm e} \simeq 385\,{\rm km\,s^{-1}}$ (Ferré-Mateu et al. 2017), for which Comerón et al. (2023) estimate $M_\bullet \simeq 5 \times 10^9\,{\rm M}_\odot$. In the hypothesis that, from the structural and kinematic point of view, NCG 1277 is representative of $z \approx 3$ quiescent galaxies of similar stellar mass, we thus construct plausible $z = 3$ $M_\bullet$-$M_\star$ and $M_\bullet$-$\sigma_{\rm e}$ correlations assuming that they have the same logarithmic slope as the corresponding $z = 0$ correlations, but normalization such that NCG 1277 lies on them. These $z = 3$ correlations are plotted in Fig. 5 together with the corresponding $z = 0$ correlations (with their intrinsic scatter) taken from Saglia et al. (2016, considering their 'CorePowerE' sample). These curves show strong evolution of the $M_\bullet$-$M_\star$ relation, but negligible evolution of the $M_\bullet$-$\sigma_{\rm e}$ relation (within the intrinsic scatter of the observed $z = 0$ relation). This behaviour of the $M_\bullet$-$M_\star$ and $M_\bullet$-$\sigma_{\rm e}$ relations of quiescent galaxies is supported by the very recent result of Newman et al. (2025), who find that the massive ($M_\star \sim 10^{11}\,{\rm M}_\odot$) gravitationally lensed quiescent galaxy MRG-M0138 at $z = 1.95$ has $M_\bullet/M_\star$ an order of magnitude higher than present-day ETGs, while being consistent with the $z = 0$ $M_\bullet$-$\sigma_{\rm e}$ relation.

In Fig. 5 we indicate with arrows the predicted evolution from $z = 3$ to $z = 0$ of our representative massive ETG in the $M_\star$-$M_\bullet$ (left panel) and $\sigma_{\rm e}$-$M_\bullet$ (right panel) planes, due to major and minor mergers (black arrows) and to envelope accretion (green arrows). The $z = 3$ BH mass is such that the initial model galaxy satisfies the $z = 3$ $M_\bullet$-$M_\star$ and $M_\bullet$-$\sigma_{\rm e}$ correlations.

The model evolution in $M_\star$ and $\sigma_{\rm e}$, which is the same as in Fig. 4, is defined in Sects. 4 and 6.3. The evolution of $M_\bullet$ due to major and minor mergers was modelled assuming that in each merger each galaxy contains a central BH, that the ratio $M_\bullet/M_\star$ is the same for both galaxies, and that the two BHs

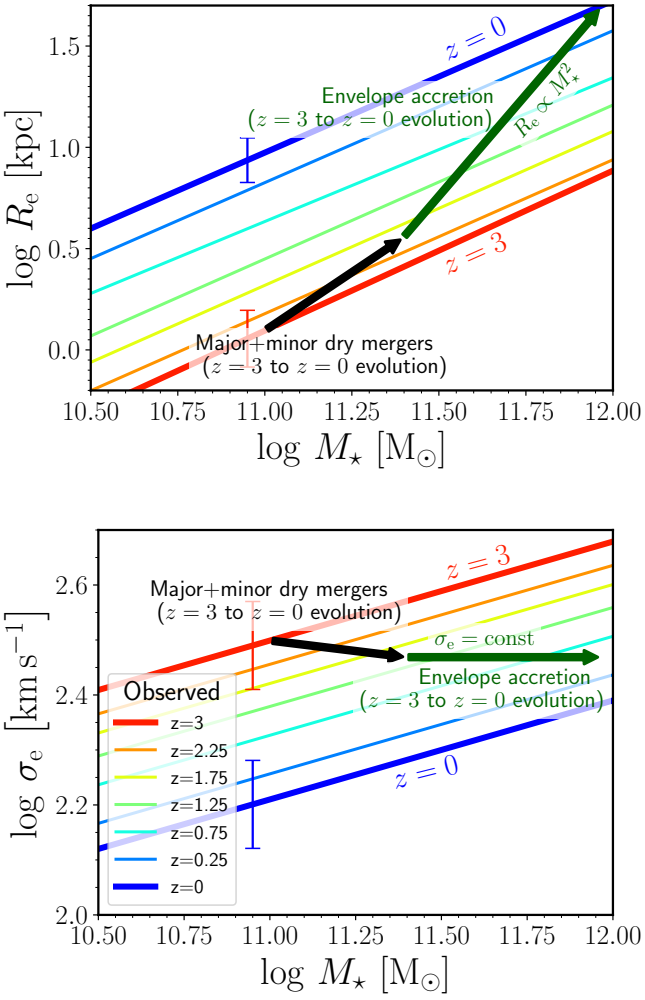

Fig. 4. ETG evolution in stellar mass, effective radius, and effective velocity dispersion, due to major and minor mergers, and envelope accretion. Same as Fig. 1, but with the addition of the potential contribution from $z = 3$ to $z = 0$ of envelope accretion (green arrows), that is diffuse accretion of loosely bound stellar systems such that $R_{\rm e}$ varies with stellar mass as $R_{\rm e} \propto M_\star^2$, while $\sigma_{\rm e}$ remains constant (see text). While the stellar mass growth attributed to major and minor mergers (black arrows) is based on observational estimates (Sect. 2.3), the stellar mass growth attributed to envelope accretion (green arrows) is chosen ad hoc so that in the upper panel the head of the green arrow lies on the observed $z = 0$ $R_{\rm e}$-$M_\star$ correlation.

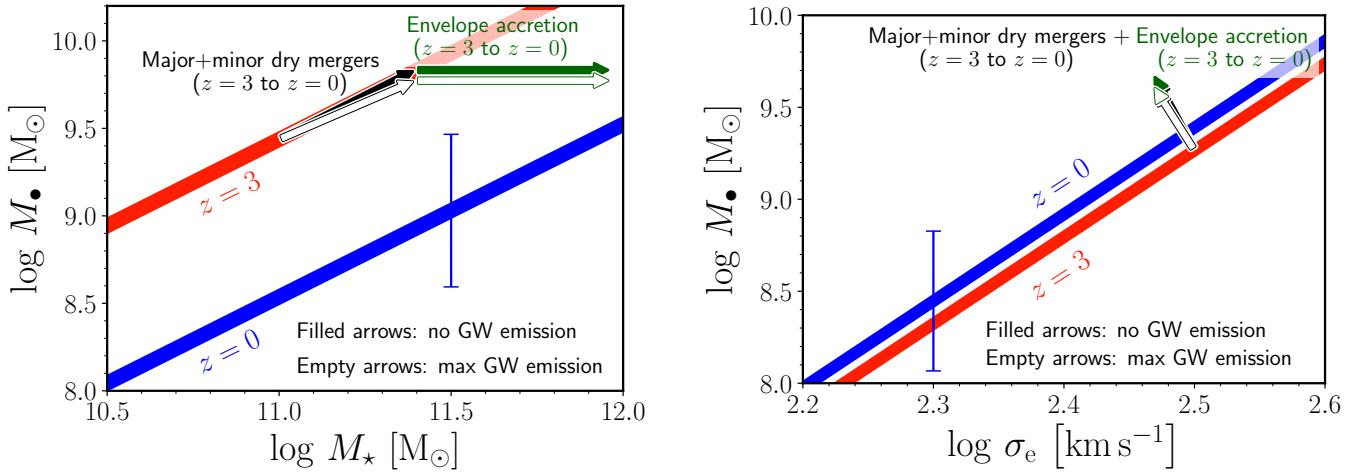

Fig. 5. ETG evolution in stellar mass, BH mass, and effective velocity dispersion, due to major and minor mergers, and envelope accretion. Left panel: The blue line is the median relation between central BH mass $M_\bullet$ and stellar mass $M_\star$ measured for observed massive $z = 0$ ETGs by Saglia et al. (2016), with the intrinsic scatter represented by the blue vertical bar. The red line is an estimate of the median relationship at $z = 3$, obtained by assuming that the logarithmic slope is the same as at $z = 0$ and that the normalization is such that the relic galaxy NCG 1277 lies on it (see text). The arrows indicate the expected evolution down to $z = 0$ of a $z = 3$ progenitor due to the combination of major and minor mergers, and envelope accretion. The filled and empty arrows correspond, respectively, to the two extreme cases of no mass loss via GW emission ($M_\bullet \propto M_\star$) and of maximal mass loss due to GW emission (see text). Right panel: Same as left panel, but for the relation between $M_\bullet$ and effective velocity dispersion σ_e. Also in this case the $z = 0$ correlation is the median obtained by Saglia et al. (2016).

coalesce forming a single BH. The mass of the BH remnant is determined by the amount of energy lost via gravitational waves (GWs), which depends on the properties of the merger (e.g. Barausse et al. 2012; Maggiore 2018). To bracket a realistic behaviour, in Fig. 5 we consider two cases: no mass loss via GWs (filled arrows) and maximal mass loss via GWs (empty arrows). In the case of no mass loss, the BH mass of the model galaxy grows proportionally to its stellar mass: $M_\bullet \propto M_\star$. In the case of maximal mass loss, we heuristically model the growth of the BH as a power law $M_\bullet \propto M_\star^{\alpha_\bullet}$, with $\alpha_\bullet = \ln(1.8)/\ln(2) \simeq 0.85$. With this choice, when the stellar mass increases by a factor of 2, the BH mass increases by a factor of 1.8, corresponding to 10% mass loss via GWs, which is the maximum expected in a BH-BH merger[6], on the basis of numerical relativity simulations (Barausse et al. 2012). Given that our model galaxy grows by a factor ≈2.5 via major and minor mergers, the final BH mass is ≈13% lower in the maximal mass loss case than in the no mass loss case, so uncertainty on the GW-driven BH mass loss has little effects for our purposes.

The fundamental assumption of the envelope accretion scenario is that the satellites are disrupted in the galaxy outskirts: if these satellites possess central BHs, these BHs (due to long dynamical-friction timescales) are not expected to reach the galactic nucleus of the main galaxy, but to become wandering BHs. We thus assume that there is no evolution of $M_\bullet$ due to envelope accretion. As a consequence, the green arrows in Fig. 5 are horizontal in the $M_\bullet$-$M_\star$ plane (left panel), because only $M_\star$ varies, and have zero length in the $M_\bullet$-σ_e plane (right panel), because neither $M_\bullet$ nor σ_e varies (see also Sect. 6.3).

[6] A factor of 2 growth in stellar mass can be due to combination of mergers with different mass ratios: for instance a single $\xi = 1$ merger or a sequence of ten mergers with satellites with stellar mass 1/10 of the initial $M_\star$. It turns out that the maximum GW-driven BH mass loss is similar in the two cases, because the maximum fractional mass loss per merger decreases for decreasing BH mass ratio (Barausse et al. 2012; Maggiore 2018).

The comparison of the arrows with the $z = 3$ ad $z = 0$ curves in Fig. 5 suggests that the combination of (major and minor) dry mergers and envelope accretion is qualitatively consistent with the hypothesized evolution of the BH scaling relations. This scenario predicts a significantly weaker growth of $M_\bullet$ than of $M_\star$ and very little evolution in the $M_\bullet$-σ_e plane. Taken at face value, the results shown in Fig. 5 indicate that the model slightly overpredicts $M_\bullet$ at $z = 0$, at given $M_\star$ or at given σ_e. However, considering the high uncertainty of the high-z BH scaling relations, this does not appear as a significant tension. Moreover, BH mergers might well be less efficient than assumed in our model, for instance as a consequence of ejection of BHs due anisotropic GW emission 'kicks' (e.g. González et al. 2007) or three-body interactions in BH merging hierarchies (e.g. Hoffman & Loeb 2007).

7.2. Dark-matter fraction

High-z quiescent galaxies tend to have lower central DM fraction than their present-day counterparts (e.g. Mendel et al. 2020). This finding is also supported by the fact that present-day relic galaxies, for which the DM can be estimated more robustly than for high-z ETGs, are very DM poor (Comerón et al. 2023). As it is usual, we define here the central DM fraction, $f_{dm,e}$, as the ratio between the DM mass and the total mass within a sphere of radius R_e (Eq. 24). While in high-z (and relic) galaxies $f_{dm,e}$ is typically lower than ≈7% (Mendel et al. 2020; Comerón et al. 2023), in normal massive present-day ETGs $f_{dm,e}$ can be higher than 20% (Cappellari et al. 2013).

During the evolution of an individual galaxy, the variation in $f_{dm,e}$ can be produced by changes of the amount of DM within a region of fixed physical size, as well as by changes of R_e. In major and minor dry mergers $f_{dm,e}$ increases for the combined effect of the redistribution of matter and increase in R_e. For instance, Nipoti et al. (2009b) find that the projected DM fraction within R_e increases by up to ≈40% in equal-mass mergers and up to a factor of 2 when the stellar mass doubles with multiple minor mergers. Hilz et al. (2013) and Frigo & Balcells (2017) find similar results

measuring the intrinsic central DM fraction in binary major and minor merger simulations. In the envelope accretion scenario, little DM is added in the central regions, but $f_{\rm dm,e}$ can increase substantially because of the increase in $R_{\rm e}$: in other words, after the build-up of the envelope $f_{\rm dm,e}$ is measured over a volume including more DM dominated regions. This is apparent from Fig. 3: in the reference model shown there, the central DM fraction raises from $f_{\rm dm,e} = 0.05$ in the initial configuration to $f_{\rm dm,e} \simeq 0.42$ in the final configuration.

Though a quantitative comparison between the observed and predicted evolution of $f_{\rm dm,e}$ appears premature, qualitatively, major and minor dry mergers, as well as envelope accretion, are promising processes to explain the increase in $f_{\rm dm,e}$ with cosmic time.

8. Conclusions

We have studied the structural and kinematic evolution of massive quiescent galaxies from $z \approx 3$ to $z \approx 0$ using state-of-the-art measurements of the evolution of the scaling relations and of the merger rates. Our main conclusions are the following.

- Major and minor mergers (with mass ratio $\xi > 1/10$) at observationally motivated rates produce, over the redshift range $0 \lesssim z \lesssim 3$, size and velocity dispersion evolution significantly weaker than that measured for ETGs, accounting only for ≈6% of the evolution in $R_{\rm e}$ and ≈40% of the evolution in $\sigma_{\rm e}$.
- The poorly constrained contribution of mini mergers (with mass ratios $\xi < 1/10$) can compensate the weak evolution induced by higher-ξ mergers, but only if these small satellites are so diffuse that they are disrupted in the galaxy outskirts, leaving the more central regions of the galaxy almost untouched. In this envelope accretion scenario, size grows fast with stellar mass (approximately as $R_{\rm e} \propto {M_\star}^2$), while $\sigma_{\rm e}$ remains essentially constant.
- A model in which quiescent galaxies grow via envelope accretion, in addition to major and minor mergers, predicts, at given stellar mass, higher central BH mass at higher redshift. This trend is consistent with the (though not so stringent) currently available observational constraints on the evolution of the $M_\bullet$-$M_\star$ and $M_\bullet$-$\sigma_{\rm e}$ relations of quiescent galaxies.
- Envelope accretion and dry mergers can also explain, at least qualitatively, the finding that the central DM fraction of quiescent galaxies increases with cosmic time.

The starting point of our investigation was highlighting quantitatively the fact that major and minor dry mergers at realistic rates are grossly unable to explain the evolution of the $R_{\rm e}$-$M_\star$ and the $\sigma_{\rm e}$-$M_\star$ relation. We have presented an idealized model of envelope accretion that shows that mini mergers can help fill the gap in the evolution of $R_{\rm e}$ and $\sigma_{\rm e}$, if the accreted satellites deposit the vast majority of their dark and luminous matter far from the galactic centre.

A potential problem is that, in order to explain the observed size evolution, our model requires that the stellar mass growth via envelope accretion is twice the growth via major and minor mergers, while there is no observational evidence, so far, of such a predominance of very small satellite accretion (see Sect. 6.3 for a discussion). However, a smaller contribution from envelope accretion would be required if the merger-driven size increase were stronger (see Sect. 3.2) or the evolution of the $R_{\rm e}$-$M_\star$ relation were weaker (see Sect. 2.1) than considered in this paper. Moreover, our model does not include the well-known effect known as progenitor bias (e.g. Franx et al. 2008), which, though expected to have a minor role for the very high-mass galaxies here considered (Fagioli et al. 2016, see also Clausen et al. 2025), would go in the direction of reducing the required mass and size growth due to envelope accretion.

Our treatment of envelope accretion is a proof of concept that can be taken as a starting point for theoretical studies aimed at modelling more quantitatively the build-up of envelopes with numerical simulations. From the observational point of view it would be beneficial to improve our knowledge of the redshift dependence of the $\sigma_{\rm e}$-$M_\star$ relation and of $f_{\rm dm,e}$ (Cannarozzo et al. 2020; Cannarozzo et al., in prep.), of the scaling relations involving BH masses (in the spirit of Newman et al. 2025 and Tanaka et al. 2025), and also, following Suess et al. (2023), of the rate and properties of mini mergers through the observation of very low-mass satellites around massive quiescent galaxies.

Acknowledgements. I am grateful to an anonymous referee for comments that helped improve the paper. The research activities described in this paper have been co-funded by the European Union – NextGenerationEU within PRIN 2022 project n.20229YBSAN – Globular clusters in cosmological simulations and in lensed fields: from their birth to the present epoch.

References

Barausse, E., Morozova, V., & Rezzolla, L. 2012, ApJ, 758, 63
Belli, S., Newman, A. B., & Ellis, R. S. 2017, ApJ, 834, 18
Binney, J., & Mamon, G. A. 1982, MNRAS, 200, 361
Binney, J., & Tremaine, S. 2008, Galactic Dynamics: Second Edition (Princeton: Princeton University Press)
Bluck, A. F. L., Conselice, C. J., Buitrago, F., et al. 2012, ApJ, 747, 34
Boylan-Kolchin, M., Ma, C.-P., & Quataert, E. 2006, MNRAS, 369, 1081
Cannarozzo, C., Sonnenfeld, A., & Nipoti, C. 2020, MNRAS, 498, 1101
Cappellari, M., di Serego Alighieri, S., Cimatti, A., et al. 2009, ApJ, 704, L34
Cappellari, M., Scott, N., Alatalo, K., et al. 2013, MNRAS, 432, 1709
Cenarro, A. J., & Trujillo, I. 2009, ApJ, 696, L43
Cimatti, A., Nipoti, C., & Cassata, P. 2012, MNRAS, 422, L62
Cimatti, A., Fraternali, F., & Nipoti, C. 2019, Introduction to Galaxy Formation and Evolution: From Primordial Gas to Present-Day Galaxies (Cambridge, UK: Cambridge University Press)
Ciotti, L., & Bertin, G. 1999, A&A, 352, 447
Ciotti, L., & van Albada, T. S. 2001, ApJ, 552, L13
Ciotti, L., Lanzoni, B., & Volonteri, M. 2007, ApJ, 658, 65
Clausen, M., Momcheva, I., Whitaker, K. E., et al. 2025, ArXiv e-prints [arXiv:2501.04788]
Comerón, S., Trujillo, I., Cappellari, M., et al. 2023, A&A, 675, A143
Conselice, C. J., Mundy, C. J., Ferreira, L., & Duncan, K. 2022, ApJ, 940, 168
Cooper, A. P., D'Souza, R., Kauffmann, G., et al. 2013, MNRAS, 434, 3348
Damjanov, I., Sohn, J., Utsumi, Y., Geller, M. J., & Dell'Antonio, I. 2022, ApJ, 929, 61
Davidzon, I., Ilbert, O., Laigle, C., et al. 2017, A&A, 605, A70
Dimauro, P., Huertas-Company, M., Daddi, E., et al. 2019, MNRAS, 489, 4135
Duan, Q., Conselice, C. J., Li, Q., et al. 2024, MNRAS, submitted [arXiv:2407.09472]
Fagioli, M., Carollo, C. M., Renzini, A., et al. 2016, ApJ, 831, 173
Fakhouri, O., & Ma, C.-P. 2010, MNRAS, 401, 2245
Ferrarese, L., & Merritt, D. 2000, ApJ, 539, L9
Ferré-Mateu, A., Mezcua, M., Trujillo, I., Balcells, M., & van den Bosch, R. C. E. 2015, ApJ, 808, 79
Ferré-Mateu, A., Trujillo, I., Martín-Navarro, I., et al. 2017, MNRAS, 467, 1929
Franx, M., van Dokkum, P. G., Förster Schreiber, N. M., et al. 2008, ApJ, 688, 770
Frigo, M., & Balcells, M. 2017, MNRAS, 469, 2184
Gebhardt, K., Bender, R., Bower, G., et al. 2000, ApJ, 539, L13
González, J. A., Sperhake, U., Brügmann, B., Hannam, M., & Husa, S. 2007, Phys. Rev. Lett., 98, 091101
Hartmann, E. A., Martín-Navarro, I., Huertas-Company, M., et al. 2025, A&A, 694, L7
Hilz, M., Naab, T., Ostriker, J. P., et al. 2012, MNRAS, 425, 3119
Hilz, M., Naab, T., & Ostriker, J. P. 2013, MNRAS, 429, 2924
Hoffman, L., & Loeb, A. 2007, MNRAS, 377, 957
Hyde, J. B., & Bernardi, M. 2009, MNRAS, 394, 1978
Ito, K., Valentino, F., Brammer, G., et al. 2024, ApJ, 964, 192
Ji, Z., Williams, C. C., Suess, K. A., et al. 2024, ApJ, submitted [arXiv:2401.00934]

Liu, R., Sonnenfeld, A., Nipoti, C., & Li, R. 2025, A&A, submitted
López-Sanjuan, C., Le Fèvre, O., de Ravel, L., et al. 2011, A&A, 530, A20
Maggiore, M. 2018, Gravitational Waves: Volume 2: Astrophysics and Cosmology (Oxford: Oxford University Press)
Magorrian, J., Tremaine, S., Richstone, D., et al. 1998, AJ, 115, 2285
Man, A. W. S., Zirm, A. W., & Toft, S. 2016, ApJ, 830, 89
Martorano, M., van der Wel, A., Baes, M., et al. 2024, ApJ, 972, 134
Mendel, J. T., Beifiori, A., Saglia, R. P., et al. 2020, ApJ, 899, 87
Mezcua, M., Pacucci, F., Suh, H., Siudek, M., & Natarajan, P. 2024, ApJ, 966, L30
Miller, T. B., van Dokkum, P., & Mowla, L. 2023, ApJ, 945, 155
Mowla, L. A., van Dokkum, P., Brammer, G. B., et al. 2019, ApJ, 880, 57
Mundy, C. J., Conselice, C. J., Duncan, K. J., et al. 2017, MNRAS, 470, 3507
Naab, T., Johansson, P. H., & Ostriker, J. P. 2009, ApJ, 699, L178
Navarro, J. F., Frenk, C. S., & White, S. D. M. 1996, ApJ, 462, 563
Nedkova, K. V., Häußler, B., Marchesini, D., et al. 2021, MNRAS, 506, 928
Newman, A. B., Ellis, R. S., Bundy, K., & Treu, T. 2012, ApJ, 746, 162
Newman, A. B., Gu, M., Belli, S., et al. 2025, ArXiv e-prints [arXiv:2503.17478]
Nipoti, C., Londrillo, P., & Ciotti, L. 2003, MNRAS, 342, 501
Nipoti, C., Treu, T., & Bolton, A. S. 2008, MNRAS, 390, 349
Nipoti, C., Treu, T., & Bolton, A. S. 2009a, ApJ, 703, 1531
Nipoti, C., Treu, T., Auger, M. W., & Bolton, A. S. 2009b, ApJ, 706, L86
Nipoti, C., Treu, T., Leauthaud, A., et al. 2012, MNRAS, 422, 1714
Oser, L., Ostriker, J. P., Naab, T., Johansson, P. H., & Burkert, A. 2010, ApJ, 725, 2312
Oser, L., Naab, T., Ostriker, J. P., & Johansson, P. H. 2012, ApJ, 744, 63
Posti, L., Nipoti, C., Stiavelli, M., & Ciotti, L. 2014, MNRAS, 440, 610
Rantala, A., Rawlings, A., Naab, T., Thomas, J., & Johansson, P. H. 2024, MNRAS, 535, 1202
Rodriguez-Gomez, V., Genel, S., Vogelsberger, M., et al. 2015, MNRAS, 449, 49
Saglia, R. P., Opitsch, M., Erwin, P., et al. 2016, ApJ, 818, 47
Schechter, P. 1976, ApJ, 203, 297
Sérsic, J. L. 1968, Atlas de Galaxias Australes (Cordoba, Argentina: Observatorio Astronomico)
Shen, S., Mo, H. J., White, S. D. M., et al. 2003, MNRAS, 343, 978
Shen, Y., Greene, J. E., Ho, L. C., et al. 2015, ApJ, 805, 96
Stockmann, M., Toft, S., Gallazzi, A., et al. 2020, ApJ, 888, 4
Suess, K. A., Kriek, M., Price, S. H., & Barro, G. 2019, ApJ, 885, L22
Suess, K. A., Williams, C. C., Robertson, B., et al. 2023, ApJ, 956, L42
Tanaka, M., Valentino, F., Toft, S., et al. 2019, ApJ, 885, L34
Tanaka, T. S., Silverman, J. D., Ding, X., et al. 2025, ApJ, 979, 215
Tortora, C., & Napolitano, N. R. 2022, Front. Astron. Space Sci., 8, 197
Trujillo, I., Ferré-Mateu, A., Balcells, M., Vazdekis, A., & Sánchez-Blázquez, P. 2014, ApJ, 780, L20
van der Wel, A., Franx, M., van Dokkum, P. G., et al. 2014, ApJ, 788, 28
van der Wel, A., Martorano, M., Häußler, B., et al. 2024, ApJ, 960, 53
van de Sande, J., Kriek, M., Franx, M., et al. 2013, ApJ, 771, 85
Vogelsberger, M., Genel, S., Springel, V., et al. 2014, MNRAS, 444, 1518
Weibel, A., de Graaff, A., Setton, D. J., et al. 2025, ApJ, 983, 11
Wright, L., Whitaker, K. E., Weaver, J. R., et al. 2024, ApJ, 964, L10